Journal of Porous Materials (2024) 31:165–175
https://doi.org/10.1007/s10934-023-01503-6

CO_2 and N_2 adsorption performance of [Rmim][NO_3] ionic liquids impregnated onto mesoporous silica at ambient pressure

Mojtaba Mirzaei[1] · Sara Hekmat Shoar[1] · Ali Sharifi[1] · M. Saeed Abaee[1]

Published online: 20 July 2023

Abstract
The CO_2 and N_2 sorption performances in neat and mesoporous silica supported ionic liquids were studied at ambient pressure. The prepared ionic liquids were four derivatives of 1-alkyl-3-methylimidazolium nitrates, where the alkyl groups were *n*-C_6H_{13}, *n*-C_8H_{17}, *n*-$C_{10}H_{21}$ or *n*-$C_{12}H_{25}$, respectively. These ionic liquids were immobilized onto porous amorphous silica and high-ordered MCM-41 via wet impregnation–vaporization method. The sorbents were characterized using ^{1}H NMR, N_2 ad/desorption, thermogravimetric analysis (TGA) and X-ray powder diffraction (XRD) methods. By passing dry CO_2 at 25 °C with 12 mL flow rate through either the neat ionic liquids or ionic liquid-loaded solid supports, [C_6mim][NO_3] and (MCM-41)-[C_{10}mim][NO_3](20) showed the highest sorption capacities, with 2.39 and 2.44 (wt%), respectively. The effects of ionic liquid loading, temperature, inlet gas flow rate, gas humidity and alkyl chain length on the CO_2/N_2 sorption capacities were also evaluated. In contrast to blank solid supports, impregnated solid supported ionic liquids lost their mesoporosity, causing a decrease in CO_2 and N_2 adsorption capacity, but an increase in CO_2/N_2 selectivity. For example, the CO_2/N_2 selectivity in (MCM-41)-[C_6mim][NO_3](20) found to be 5.6, but by increase of the ionic liquid portion in (MCM-41)-[C_6mim][NO_3](50), the CO_2/N_2 selectivity increased to 17.2, proving that the ionic liquid plays a decisive role in selective adsorption of CO_2.

Keywords Ionic liquid · CO_2 adsorption · N_2 adsorption · Mesoporous solid support · CO_2/N_2 selectivity

1 Introduction

The huge amounts of CO_2 production is the main factor responsible for global warming [1]. The most common way for CO_2 removal is based on chemisorption of CO_2 in aqueous alkanolamine solutions such as monoethanolamine (MEA), methyldiethanolamine (MDEA) and diethanolamine (DEA). However, this method suffers from some problems like loss of solvent during regeneration of the alkanolamine solutions, equipment corrosion and high energy consumption [2]. Room Temperature Ionic Liquids (RTILs) are a group of compounds consisted of ions only, often remaining liquid over a wide range of temperature even below 25 °C. The unique properties of RTILs as being inflammable, noncorrosive and electrically conductive, and possessing high thermal stability, negligible vapour pressure and tuneable physiochemical properties, introduce them as good surrogates to conventional solvents [3]. The notable point about ionic liquids (ILs) is that their inherent features, such as hydrophobicity/hydrophilicity, viscosity and melting point can be arbitrary tuned by altering the cation or the anion counterpart, to tailor them for desired applications. Their tuneable properties along with insolubility in gases have guided researchers to use them as suitable alternative solvents for acid gas removal.

Blanchard was the pioneer to illustrate the ability of ILs in CO_2 absorption [4]. Subsequently numerous studies were reported on the solubility of CO_2 and other gases in ILs. It was also observed that ILs with fluorine containing anions have higher affinities for CO_2, and by an increase in the alkyl chain length on the cation part, the absorption capacities also increase [5]. The evaluation of CO_2 absorption mechanism in ILs having no additional functional groups showed that the CO_2 molecules only fill the spaces created by arrangement of the ions, and that there are only weak Lewis acid–Lewis base interactions between CO_2 and the anions [6]. The first Task-Specific Ionic Liquid (TSIL) introduced by Bates was an imidazolium-based IL, containing an amino group on the cation ring, being able to absorb CO_2 more effectively than

✉ Mojtaba Mirzaei
mirzaei@ccerci.ac.ir

[1] Chemistry and Chemical Engineering Research Center of Iran, P.O. Box 14335-186, Tehran, Iran

traditional RTILs by passing CO_2 stream under atmospheric pressure [7].

Considering the problems associated with the use of neat ILs along with the ease of working with solid powder, researchers were convinced to use adsorbents produced by impregnation of ILs on solid substrates, as opposed to the use of expensive and viscose neat ILs [8]. Consequently, solid supported ILs found high attractions for many applications in catalysis, heavy metals absorption from waste water and acid-gas removal from natural gas streams. The supported Ionic Liquids (SILs) technology is a new route to make a liquid containing solid material, obtained by impregnating or grafting a thin film of ILs onto the solid supports. The best advantage of this approach is the selection of appropriate anions and cations in the IL structure, whose specific properties are transferred to the surface of the solid support [9]. Ren introduced amino acid-based ILs supported on silica gel as good adsorbents for CO_2 [10]. Zhu et al. have also synthesized and immobilized imidazolium and phosphonium ILs onto porous silica surface and reported that the bare silica adsorbs CO_2 better than ILs modified silica, and that the CO_2 adsorption capacities of sorbents prepared via grafting methods were more than those prepared by impregnation methods [11]. Yang immobilized [N1111][Gly] into porous PMMA (polymethyl methacrylate) and found that the PMMA impregnated with 50 wt% of [N1111][Gly] exhibited the best CO_2 adsorption performance. The highest CO_2 adsorption capacity of 2.14 mmol/g was obtained in PMMA-50 at 35 °C and at ambient pressure [12].

We recently reported the CO_2 sorption of the neat and silica supported 1-butyl-3-methylimidazolium with eight different anions at ambient pressure, where the anions were $[BF_4]^-$, $[PF_6]^-$, $[Tf_2N]^-$, $[TfO]^-$, $[HSO_4]^-$, $[NO_3]^-$, $[SCN]^-$ and $[N(CN)_2]$, respectively. The results showed that by continuous passing of dry CO_2 through the sorbents, [Bmim][N(CN)$_2$] and SiO_2-[Bmim][HSO_4)](50) had the highest sorption capacities. We also found that by increasing the IL portion (x) in SiO_2-[Bmim][NO_3](x), the CO_2/CH_4 selectivity increased. For instance, SiO_2-[Bmim][NO_3] (33) and SiO_2-[Bmim][NO_3](50) can adsorb CO_2 6.36 and 9.67 times more than CH_4, respectively [13, 14]. Due to having uniform arrangement of hexagonally shaped pores, mesoporous MCM-41 is particularly interesting as being a solid support for immobilization of ILs onto its mesoporous structure, due to having large pore volume and high surface area [15]. As we reported recently [13, 14], and also due to economic and environmental perspectives, ILs with nitrate ion as the anion counterpart may meet our expectations.

In the present study, an impregnation method was used to immobilize the four synthesized ILs on amorphous silica and ordered mesoporous MCM-41, and subsequently their CO_2 and N_2 adsorption capacities were compared to the neat four IL analogues. In other words, we planned to study the effect of ILs in CO_2/N_2 sorption selectivities. Thus, four 1-alkyl-3-methylimidazolium nitrate ILs with different alkyl lengths were prepared and immobilized onto silica-based supports via an impregnation–vaporization method. Subsequently, the CO_2 and N_2 adsorption capacities of the bare and IL-loaded silica-based supports were measured and the effects of factors such as temperature, inlet gas flow rate, humidity, along with IL-loadings were evaluated.

2 Experimental

2.1 Materials

N-Methylimidazole (98%), silica-60 (0.02–0.04 mm), hydrochloric acid (HCl, 37% aq), sodium nitrate ($NaNO_3$, 98%), silver nitrate ($AgNO_3$, 99.8%), phosphorus pentoxide (P_2O_5, 98%), 1-chlorohexane ($C_6H_{13}Cl$, 98%), 1-chlorooctane ($C_8H_{17}Cl$, 98%), 1-chlorodecane ($C_{10}H_{21}Cl$, 98%), 1-chlorododecane ($C_{12}H_{25}Cl$, 98%), sulphuric acid (H_2SO_4, 98%) and organic solvents (acetonitrile, ethyl acetate, ether, dichloromethane, acetone, anhydrous ethanol and chloroform) were all obtained from Merck Company. Sodium hydroxide (NaOH, 98%), ammonium hydroxide (NH_4OH, 25% aq) and tetraethyl orthosilicate (TEOS, 98%) were purchased from Acros Organics. Carbon dioxide (CO_2, ≥ 99.995%) and nitrogen (N_2, ≥ 99.995%) were supplied by Pars Gas Company.

2.2 Synthesis of [Rmim][NO_3] ILs

1-Hexyl-3-methylimidazolium nitrate ([C_6mim][NO_3]), 1-methyl-3-octylimidazolium nitrate ([C_8mim][NO_3]), 1-decyl-3-methylimidazolium nitrate ([C_{10}mim][NO_3]) and 1-dodecyl-3-methylimidazolium nitrate ([C_{12}mim][NO_3]) were prepared via a two-step synthesis. For this, the corresponding 1-chloroalkane (slightly excess) was treated with 1-methylimidazole to obtain the crude [Rmim][Cl] (Scheme 1).

The impurities (unreacted starting materials) were removed from the mixture by solvent extraction to obtain the required [Rmim][Cl] [16]. Next, the resulting [Rmim][Cl] salts were treated with $NaNO_3$ in dichloromethane to undergo ionic exchange. The remaining [Rmim][Cl] impurities were removed by passing a dichloromethane solution of the impure [Rmim][NO_3] through the silica column, until no precipitation of AgCl was observed by addition of $AgNO_3$ solution to the filtrate. After removal of dichloromethane, the synthesised IL was dried under vacuum for 6 h to obtain the desired ILs as light yellow viscose liquids with a purity of ≥ 98% [17], which were protected from moisture. The physical properties of the ILs are shown in Table 1. It should be noted that [C_{12}mim][NO_3] IL is solid at 25 °C.

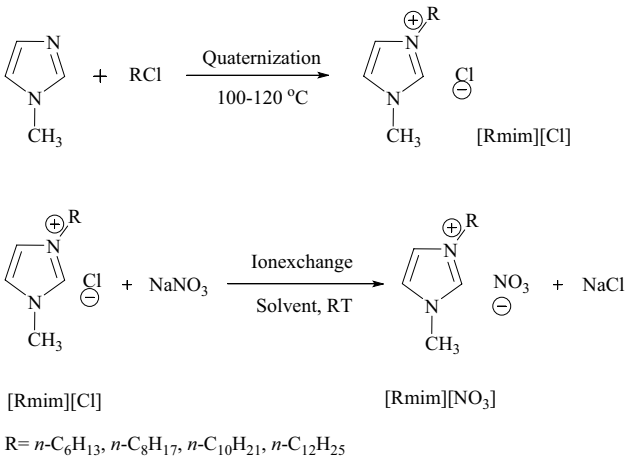

Scheme 1 Synthesis of [Rmim][NO_3] ILs

2.3 Synthesis of ordered mesoporous silica (MCM-41)

We synthesized MCM-41 according to the reported method [15] using tetraethyl orthosilicate (TEOS) as the silica source, 1-tetradecyl-3-methylimidazolium chloride [C_{14}mim][Cl] as the template, hydrochloric acid and water. The molar composition of the solution was 0.05, 0.01, 1.2, 2.6 and 7.2 for TEOS, [C_{14}mim][Cl], NH_4OH, C_2H_5OH and H_2O, respectively. Thus, [C_{14}mim][Cl] (3.15 g) was added to a room temperature mixture of water (130 mL) and ethanol (16 mL) in a 250 mL conical vessel. After completion of the dissolution, ammonia (11 mL, 25% aq) was added dropwise to the reaction solution. Then TEOS (11.2 mL) was added dropwise to the solution within 25 min. After 3 h mixing at room temperature, the resulting white suspension was transferred into a stainless steel reactor and kept at 120 °C for 20 h. Then, the solid was filtered and washed with 200 mL of deionized water and dried in an oven at 110 °C for 12 h to obtain MCM-41, which was calcinated in air at 600 °C for 6 h at 5 °C/min heating rate.

2.4 Activation of amorphous SiO_2

As we reported before [13], the amorphous silica used in the present study was activated by being refluxed and stirred in HCl (6 M). The resulting suspended SiO_2 powder in acidic solution was filtered and washed several times with distilled water until the pH of the solution was adjusted in the range of 6–7. Next, the resulting wet solid was dried in 130 °C for 10 h to give the desired activated porous silica support, which was kept in a desiccator containing a dehumidifier agent.

2.5 Synthesis of IL-loaded SiO_2 or MCM-41

The ILs were immobilized onto amorphous silica and ordered mesoporous MCM-41 using an impregnation–vaporization method [18] (Scheme 2).

These solid adsorbents were symbolized as SiO_2-IL(x) and (MCM-41)-IL(x), where x indicates the mass percentage of IL in the adsorbents. For example, for the preparation of the (MCM-41)-[C_6mim][NO_3](20), 1.0 g of [C_6mim][NO_3] was dispersed in 20 mL of absolute ethanol for 30 min. Then the activated MCM-41 (4.0 g) was added to the solution and the mixture was stirred under reflux for 6 h. After removal of the bulk of the solvent, the wet powder was dried at 80 °C under 10 mmHg pressure for 6 h. The resulting IL-loaded solid supports were kept dry in a desiccator containing a dehumidifier agent. The exact amount of the stabilized IL on SiO_2-IL(x) and (MCM-41)-IL(x) was obtained by TGA (Table 2).

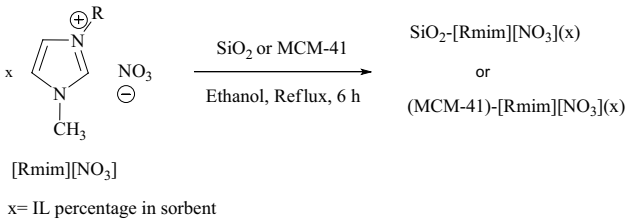

Scheme 2 Preraration of SiO_2-[Rmim][NO_3](x) and (MCM-41)-[Rmim][NO_3](x) via impregnation method

Table 1 Density and viscosity of the synthesized ILs

Ionic liquids	Density (kg/m^3)			Viscosity (Pa s)		
	25 °C	40 °C	50 °C	25 °C	40 °C	50 °C
[C_6mim][NO_3]	1073.02	1063.70	1057.70	0.0622	0.0322	0.0228
[C_8mim][NO_3]	1059.76	1050.29	1044.05	0.0300	0.0179	0.0134
[C_{10}mim][NO_3]	1036.55	1027.30	1021.14	1.0847	0.3898	0.2207
[C_{12}mim][NO_3]	–	1006.14	1000.00	–	0.7993	0.4093

Standard uncertainty u are $u(d) = 0.01$ kg/m^3, $u(V) = 0.0001$ Pa s

Table 2 Pore characteristics of SiO_2-[C_6mim] [NO_3](x) and (MCM-41)-[C_6mim][NO_3](x)

Sorbents	IL/sorbent[a]	$V_ϱ$	$A_ϱ$	$D_ϱ$
		(cm^3/g)[b]	(m^2/g)[c]	(nm)[d]
SiO_2 (amorphous)	0	0.672	351.70	7.66
SiO_2-[C_6mim][NO_3](20)	19.85	0.381	206.38	7.33
SiO_2-[C_6mim][NO_3](30)	30.2	0.272	132.36	8.29
SiO_2-[C_6mim][NO_3](40)	40.03	0.043	16.24	10.18
SiO_2-[C_6mim][NO_3](50)	49.38	0.001	1.12	3.84
MCM-41	0	0.733	1177.80	2.49
(MCM-41)-[C_6mim][NO_3](20)	21.20	0.173	217.74	3.17
(MCM-41)-[C_6mim][NO_3](30)	31.74	0.048	150.11	12.70
(MCM-41)-[C_6mim][NO_3](40)	40.85	0.024	23.25	29.16
(MCM-41)-[C_6mim][NO_3](50)	51.14	0.020	8.73	11.22

[a]Actual IL/sorbent in solid sorbent

[b]Total pore volume

[c]Specific surface area

[d]Average pore diameter

2.6 Characterizations of the neat and SiO_2 or MCM-41 supported ILs

The ILs were characterized as $CDCl_3$ or DMSO-d6 solutions by ^{1}H NMR spectroscopy (Bruker Advance spectrometer, 500 MHz). Density and viscosity of the ILs were measured with densitometer model DEM-5000-Anton paar (± 0.01 kg/m^3) and Viscometer model Anton paar SVM 3000 (± 0.0001 Pa S). The water contents of the ILs were measured by Karl-Fischer (KF-Coulometer 831). The water content of CO_2 flue was measured by Vaisala humidity sensor (VAISALA HMP63). The total chloride contents of the ILs were determined potentiometrically using a chloride ion selective electrode (ISE) connected to a pH meter (Philips PW 9420). Thermogravimetric Analysis (TGA) of the pure ILs, SiO_2-ILs(x) and (MCM-41)-ILs(x) were performed from 25 to 900 °C using a NETZSCH TG 209 F1 Iris instrument under N_2 atmosphere with a heating rate of 10 °C/min. The N_2 ad/desorption isotherms were performed to earn pore size distribution, specific surface area and porosity of the solid sorbents, using BELSORP-mini II Analyser. Prior to analysis, samples were degassed at 100 °C and 10^{-3} bar for 10 h. The total pore volume was evaluated from adsorbed N_2 amount at a relative pressure of $P/P_0 = 1$. The pore size distributions were concluded from the desorption diagram using Barrett-Joyner-Halenda (BJH) analysis. The X-ray powder diffraction (XRD) data for the bare and IL-loaded MCM-41 were obtained using a powder diffractometer DRON-4-02 apparatus (Burevestnik, Russia) with the monochromatic CuKα emission (λ¼41.54178 Å) and nickel filter. Interplanar distances were calculated using the Bragg diffraction equation. The sorbents were scanned from Bragg angle (2θ) of 10° to 70° [19].

2.7 Experimental procedure for CO_2 and N_2 sorption

The experimental setup used in this study is similar to that we reported before [13]. The sorption process was carried out in a T-formed or U-shaped glass reactor for liquid and solid state sorbents. The Mass Flow Controller (Smart MFC Brooks, SLA5850, (± 0.01 mL/min) was used to stabilize the gas inlet flow rate to the reactor at a certain flow rate. The mass gain of sorbents was measured with an electronic balance (± 0.0001 g). The sorption capacity was measured at 25, 40 or 50 °C by bubbling the CO_2 or N_2 into the neat ILs and passing through the solid adsorbents. The CO_2-enriched sorbents were degassed under 10 mmHg pressure at 70 °C. The CO_2 ab/adsorption capacity of the neat and solid supported ILs were measured at atmospheric pressure by passing dry CO_2 with a flow rate of 12 mL/min at 25 °C.

To calculate CO_2 absorption capacities of neat IL, 2 mL of IL was transferred to a T-shaped glass reactor and warmed at 70 °C under 10 mmHg pressure for 90 min to remove any existing humidity or volatile contents. After cooling to room temperature, the glass reactor was inserted into a water bath (Open Bath\circulation Huber CC-K20), which had been preheated at 25, 40 or 50 °C. After stabilization of flow rate and the temperature at the desired values, first CO_2 was entered to a P_2O_5-packed column to remove the existing humidity. Then the resulting dry CO_2 was entered to a T-shaped glass reactor and was blown through a neat IL and vented from the output valve. In order to measure the amounts of absorbed CO_2 at certain times, the valves

were closed and the reactor weight gain was measured with an electronic balance (±0.0001). The adsorption process continued until no additional mass gainobserved. The CO_2 adsorption capacities of the SiO_2-ILs(x) and (MCM-41)-ILs(x) were measured under the conditions similar to those used for the neat ILs, unless a U-shaped glass reactor was used instead of the T-shaped one. To recycle the adsorbent, the CO_2- or N_2-enriched sorbent was located into a 70 °C water bath and degassed under 10 mmHg pressure until no weight decrease was observed for the reactor.

3 Results and discussion

3.1 Characterization of the Ils

The structures of the [Rmim][NO_3] ILs were confirmed by their ^{1}H NMR spectroscopic data, shown in the supplementary information (Table S1). The water contents of the ILs were less than 550 ppm, while the chloride anion [Cl^-] impurity was between 2000 and 3000 ppm (Table S1). The density and viscosity values of the neat ILs are listed in the Table 1.

3.2 Characterization of synthesized SiO_2-ILs(x) or (MCM-41)-ILs(x)

The activated amorphous silica had specific surface area of 351.70 m^2/g, total pore volume of 0.79 cm^3/g and average pore diameter of 8.53 nm. As shown in Table 2, the specific surface area of the SiO_2-[C_6mim][NO_3](x) adsorbents decreased from 351 m^2/g in bare silica to 206.38, 132.36, 16.24 and 1.11 m^2/g for x equal to 20, 30, 40 and 50, respectively. The reduction of surface area revealed that the pores were filled with [C_6mim][NO_3] molecules. The pore size distribution showed that much of the pores diameters are between 2 and 10 nm, indicating that the majority of the pores are mesopore. As indicated in Fig. 1, the bare silica and SiO_2-[C_6mim][NO_3](x) showed similar type IV N_2 adsorption isotherms and type A hysteresis loops, supporting that the SiO_2-[C_6mim][NO_3](x) has mesoporous structure with cylindrical shape of pores. It was noted for SiO_2-[C_6mim][NO_3](x), when the IL-loading rises to 50 wt%, no pore structure was seen and the hysteresis vanishes completely. Table 2 shows a reduction of the total pore volume in SiO_2-[C_6mim][NO_3](x) from 0.38 cm^3/g in x = 20 to 0.27, 0.04 and 0.001 cm^3/g, respectively, in x equal to 30, 40 and 50, while by the increase of IL portion in SiO_2-[C_6mim][NO_3](x), the average pore diameter increased from 7.33 nm in x = 20, to 8.29 and 10.18 nm in x = 30 and 40, respectively. As x rises to 50, the average pore diameter decreases again. It was found from the pore size distribution in Fig. 1

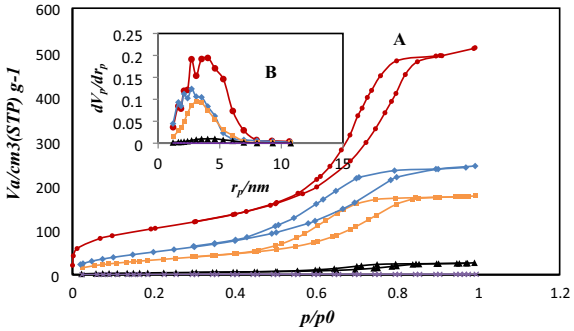

Fig. 1 **A** N_2 Adsorption–desorption isotherms and **B** BJH pore size distribution of SiO_2-[C_6mim][NO_3](x) with x = 0 (●), 20 (♦), 30 (■), 40 (▲) and 50 (×)

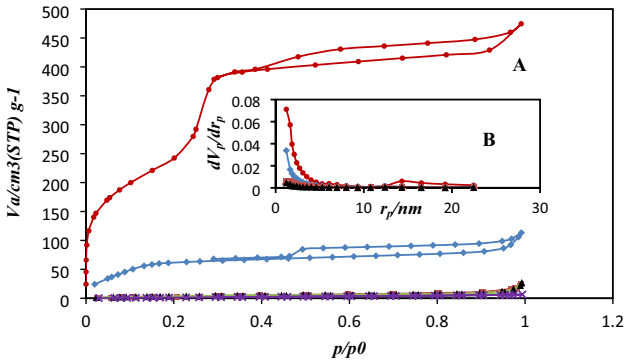

Fig. 2 **A** N_2 Adsorption–desorption isotherms and **B** BJH pore size distribution of (MCM-41)-[C_6mim][NO_3](x) with x = 0 (●), 20 (♦), 30 (■), 40 (▲) and 50 (x)

that the mesoporosity in SiO_2-IL(x) would be preserved up to x < 50.

Experiments showed that MCM-41 as an high-ordered mesoporous silica had specific surface area of 1177.80 m^2/g, total pore volume of 0.733 cm^3/g and average pore diameter of 2.49 nm. As shown in Table 2, the specific surface area of (MCM-41)-[C_6mim][NO_3](x) adsorbents decreased from 1177.8 m^2/g in bare MCM-41 to 217.74, 150.11, 23.25 and 8.73 m^2/g for x equal to 20, 30, 40 and 50, respectively. Supporting that the pores were occupied by [C_6mim][NO_3] molecules. The pore size distribution in (MCM-41)-[C_6mim][NO_3](x) showed that most of the pores have diameters between 2 and 10 nm, showing that the majority of the pores are mesoporous (Fig. 2). As seen in Fig. 2, the bare MCM-41 and (MCM-41)-[C_6mim][NO_3](20) represented similar isotherms of type IV and the cylindrical form of the pores was approved by the existence of the hysteresis type A.

Table 2 shows that the total pore volume (V_p) in (MCM-41)-[C_6mim][NO_3](x) decreased from 0.173 cm^3/g in x = 20 to 0.048, 0.024 and 0.020 cm^3/g in x equal to 30, 40 and 50, respectively, while by increasing the IL portion

in (MCM-41)-[C_6mim][NO_3](x), the average pore diameter increased from 3.17 nm in x = 20 to 12.70 and 29.16 nm in x = 30 and 40, respectively. When x was increased to 50, the average pore diameter decreased to 11.22 nm.

As seen in Fig. 3 and summarized in Table 2, the actual amounts of the IL impregnated on silica and MCM-41 supports were determined by TGA. The TGA spectra of the adsorbents showed that SiO_2-[C_6mim][NO_3](40) and (MCM-41)-[C_6mim][NO_3](30) had the lowest (0.075%) and the highest (5.8%) deviation from the standard, respectively, conveying that parts of the solid powder were wasted through immobilization process.

The X-ray diffraction pattern of the synthesized MCM-41 with new template after calcination is shown in Fig. 4. It appears that there are three diffraction peaks at 2.42, 4.06 and 4.56 2θ, suggesting that the bare MCM-41 and (MCM-41)-[C_6mim][NO_3](20) have well-ordered hexagonal arrangements. In contrast, at x = 30, the XRD patterns intensity diminished and tended to zero at x ≥ 40, perhaps due to the occupation of the majority of the cavities by the IL molecules.

3.3 CO_2 sorption process

The absorption capacities of the neat ILs were measured at 25, 40 and 50 °C by passing dry CO_2 with a 12 mL/min flow rate at ambient pressure through the absorbents. The results in Table 3 show that [C_6mim][NO_3] and [C_{12}mim][NO_3] with 2.39 wt% and 0.5 wt%, had respectively the highest and the lowest CO_2 absorption capacities. As shown in Fig. 5, the saturation time for [C_6mim][NO_3] was 1500 min, while it was 100 min for [C_{12}mim][NO_3]. The CO_2 solubility capacities of the four ILs at 25 °C could be stated in the order of [C_6mim][NO_3] > [C_{10}mim][NO_3] > [C_8mim][NO_3] > [C_{12}mim][NO_3]. The CO_2 adsorption processes of

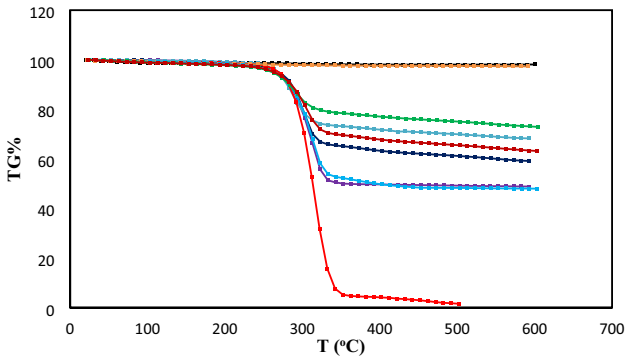

Fig. 3 TGA curves of [C_6mim][NO_3] (■), SiO_2-[C_6mim][NO_3](x) with x = 0 (■), 30 (■), 40 (■), 50 (■) and (MCM-41)-[C_6mim][NO_3](x) with x = 0 (■), 30 (■), 40 (■), 50 (■) (N_2 atmosphere, heating rate of 20 °C/min)

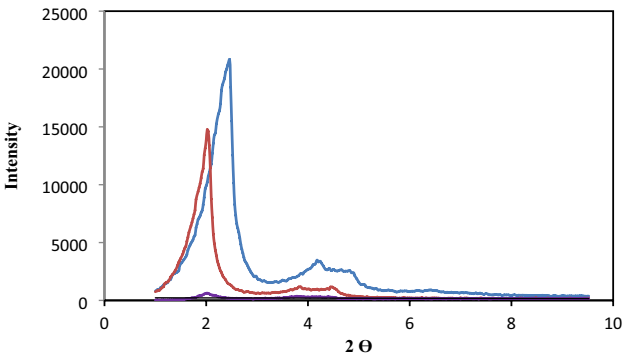

Fig. 4 XRD pattern of (MCM-41)-[C_6mim][NO_3](x) with x = 0 (–), 20 (–) and 30 (–)

the SiO_2-IL(x) adsorbents were conducted in a U-Shaped glass reactor at 25 °C by passing dry CO_2 stream with a flow rate of 12 mL/min. As shown in Fig. 5, SiO_2-[C_6mim][NO_3](50) and SiO_2-[C_{12}mim][NO_3](50) with 1.50 and 1.05

Table 3 CO_2 sorption capacity of the sorbents by passing the dry CO_2 with a flow rate of 12 mL/min

Sorbents	CO_2 (wt%)[a]		
	25 °C	40 °C	50 °C
[C_6mim][NO_3]	2.39	1.75	1.28
SiO_2 (amorphous)	2.20	1.55	0.95
SiO_2-[C_6mim][NO_3](20)	2.10	1.52	1.12
SiO_2-[C_6mim][NO_3](30)	1.81	1.25	0.89
SiO_2-[C_6mim][NO_3](40)	1.62	1.18	0.85
SiO_2-[C_6mim][NO_3](50)	1.50	1.10	0.65
MCM-41	3.58	2.61	1.78
(MCM-41)-[C_6mim][NO_3](20)	2.30	1.68	1.33
(MCM-41)-[C_6mim][NO_3](30)	1.95	1.42	1.08
(MCM-41)-[C_6mim][NO_3](40)	1.73	1.35	0.98
(MCM-41)-[C_6mim][NO_3](50)	1.55	1.09	0.81
[C_8mim][NO_3]	1.49	1.34	0.83
SiO_2-[C_8mim][NO_3](20)	2.07	1.05	0.65
SiO_2-[C_8mim][NO_3](50)	1.47	–	–
(MCM-41)-[C_8mim][NO_3](20)	2.35	–	–
(MCM-41)-[C_8mim][NO_3](50)	1.53	–	–
[C_{10}mim][NO_3]	1.44	1.21	0.89
SiO_2-[C_{10}mim][NO_3](20)	1.88	1.45	0.96
SiO_2-[C_{10}mim][NO_3](30)	1.68	1.39	0.85
SiO_2-[C_{10}mim][NO_3](40)	1.45	1.19	0.77
SiO_2-[C_{10}mim][NO_3](50)	1.36	1.12	0.58
(MCM-41)-[C_{10}mim][NO_3](20)	2.44	1.93	1.44
(MCM-41)-[C_{10}mim][NO_3](50)	1.42	–	–
[C_{12}mim][NO_3]	0.50	1.15	0.71
SiO_2-[C_{12}mim][NO_3](20)	1.59	1.28	0.88
SiO_2-[C_{12}mim][NO_3](50)	1.05	0.63	0.45

[a]Standard uncertainty u are $u(CO_2) = 0.03$ wt%

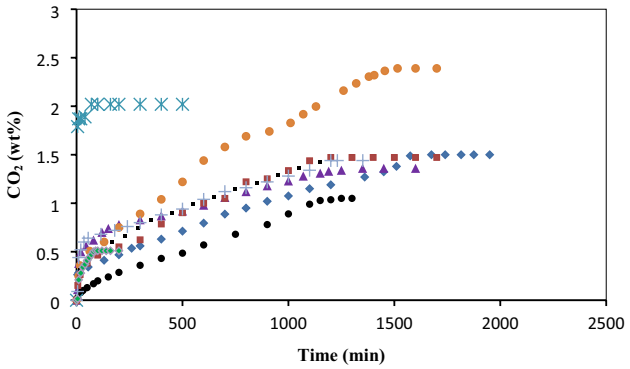

Fig. 5 CO_2 sorption diagram of $[C_6mim][NO_3]$ (●), $[C_8mim][NO_3]$ (−), $[C_{10}mim][NO_3]$ (+), $[C_{12}mim][NO_3]$ (♦), bare SiO_2 (Ж), SiO_2-$[C_6mim][NO_3](50)$ (♦), SiO_2-$[C_8mim][NO_3](50)$ (■), SiO_2-$[C_{10}mim][NO_3](50)$ (▲) and SiO_2-$[C_{12}mim][NO_3](50)$ (●) at 25 °C by passing dry CO_2 with a flow rate of 12 mL/min

wt% weight gain had the highest and the lowest adsorption capacities among the four SiO_2-$[Rmim][NO_3](50)$ adsorbents, respectively. The CO_2 solubility capacities of the four ILs-loaded silica adsorbents at 25 °C could be written in the order of SiO_2-$[C_6mim][NO_3](50) > SiO_2$-$[C_8mim][NO_3](50) > SiO_2$-$[C_{10}mim][NO_3](50) > SiO_2$- \$[C_{12}mim][NO_3](50)$.

Considering the effect of the solid support on the adsorption phenomenon, the CO_2 adsorption capacities of some IL-loaded MCM-41 adsorbents were investigated as well (Fig. 6). The ILs and the process conditions were the same as those used for SiO_2-IL(x). As expected, due to larger surface area, the CO_2 adsorption capacities in (MCM-41)-IL(x) were higher than those of the corresponding SiO_2-IL(x), while in the cases of (MCM-41)-based adsorbents, the required time for saturation were less than the corresponding SiO_2-based counterparts. For example, the CO_2 adsorption capacity in bare amorphous silica with a surface area of 351 m^2/g was 2.20%, when dry CO_2 was passed through with a flow rate of 12 mL/min within 170 min. In contrast, the bare MCM-41 with a surface area of 1177 m^2/g earned 3.58 wt% weight gain within 50 min gas passage under similar conditions.

This pattern was also observed for SiO_2-IL(x) and (MCM-41)-IL(x). For example, the CO_2 adsorption capacity of SiO_2-$[C_{10}mim][NO_3](20)$ was 1.88 wt%, while it was 2.44 wt% in the case of (MCM-41)-$[C_{10}mim][NO_3](20)$.

Figure S1 shows the desorption process for the neat and solid supported ILs. The CO_2-enriched sorbents easily lose the adsorbed CO_2 in less than 30 min under 10 mmHg pressure. The easy regeneration process is due to the lack of a strong bond between the gas and the sorbent molecules.

4 Affecting factors on CO_2 sorption capacity

4.1 Temperature

In most cases, by temperature increase, the solubilities of gases in solvents decrease. In the present article, we were curious to know if this also applies to the ILs under our conditions. For this purpose, the absorption capacities of the neat ILs were evaluated at 25, 40 and 50 °C. The results were reported in Table 3 and showed that by an increase in temperature, the CO_2 absorption capacities of neat ILs decrease. For example at 25 °C by passing dry CO_2 with a flow rate of 12 mL/min, $[C_6mim][NO_3]$ absorbed 2.39 wt%, but by increasing the temperature to 40 and 50 °C, the absorption capacity decreased to 1.75 wt% and 1.28 wt%, respectively (Fig. 7). There was an exception for $[C_{12}mim][NO_3]$, which is solid at 25 °C and its absorption capacity at 40 °C would be higher than that of at 25 °C. However, by increasing the temperature to 50 °C, the absorption capacity

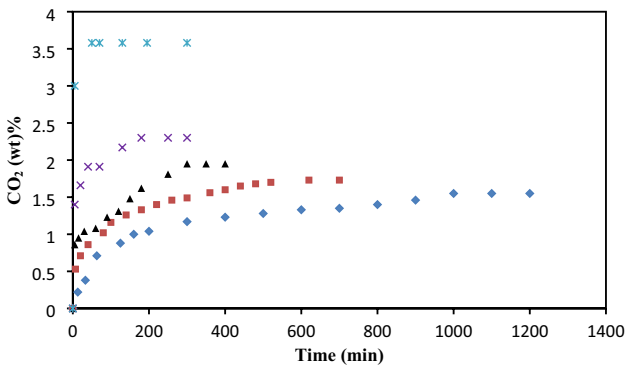

Fig. 6 CO_2 adsorption plot of (MCM-41)-$[C_6mim][NO_3](x)$ with x = 0 (Ж), 20 (×), 30 (▲), 40 (■) and 50 (♦) at 25 °C by passing dry CO_2 with a flow rate of 12 mL/min

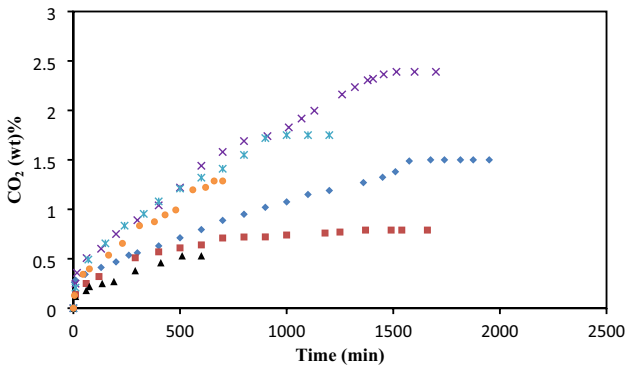

Fig. 7 CO_2 sorption diagram of $[C_6mim][NO_3]$ at 25 °C(×), 40 °C (Ж), 50 °C (●) and SiO_2-$[C_6mim][NO_3](50)$ at 25 °C(♦), 40 °C (■) and 50 °C (▲) by passing dry CO_2 with a flow rate of 12 mL/min

decreased again. This relation between the temperature and gas adsorption capacities was also seen in SiO_2-ILs(x) and (MCM-41)-ILs(x). For example, the CO_2 adsorption capacity of SiO_2-[C_{10}mim][NO_3](20) at 25 °C was 1.88 wt%, but by increase of the temperature to 40 and 50 °C, the adsorption capacities decreased to 1.45 and 0.96 wt%, respectively. This trend was also observed in (MCM-41)-IL(x)/ For instance, (MCM-41)-[C10mim][NO_3](20) was capable of adsorbing 2.44 wt% dry CO_2 at 25 °C, while by rising the temperature to 40 and 50 °C, the adsorption capacities decreased to 1.93 and 1.44 wt%, respectively. As would be seen for neat ILs (Fig. S2), there was an approximately linear correlation between the temperature and the gas adsorption capacities for SiO_2-ILs(x) and (MCM-41)-ILs(x) (Fig. S3).

4.2 Humidity

The ILs used in this study are able to absorb moisture from the environment. This persuaded us to see the moisture effect in the sorption capacities of the neat and SiO_2- and MCM-41 supported ILs. For this purpose, the P_2O_5-packed column was removed from the operational setup and a gas stream with 400 ppm water content was allowed to enter the reactor. Similar to dry flue gas, the CO_2 sorption capacities of the sorbents were measured at 25, 40 and 50 °C by passing the wet gas with a flow rate of 12 mL/min. As seen in Table 4, by passing dry CO_2 at 25 °C, [C_6mim][NO_3] weight gain was 2.39 wt%, but under the same conditions, the weight gain raised to 3.20 wt% when wet CO_2 was passed through the setup. According to Table 4, the results showed that, the gas adsorption capacities of the SiO_2-ILs and (MCM-41)-ILs increased by passing the wet gas through the solid powders, similar to the observation for the neat ILs. For example, the dry CO_2 adsorption capacities of SiO_2-[C_6mim][NO_3](50) at 25 °C was 1.51 wt%, while by passing wet CO_2, the adsorption capacities increased to 2.39 wt%. Due to hydrophilic nature of the ILs used, the absorbed water from the flue gas comes into equilibrium with CO_2, resulting in an increase in CO_2 sorption capacity [13, 14].

Table 4 Comprative gas sorption capacity of the sorbents by passing wet and dry CO_2 in 12 mL/min flow rate

Sorbents	CO_2 (wt%)[a]	
	Dry	Wet
[C_6mim][NO_3]	2.39	3.20
SiO_2	2.02	2.57
[C_8mim][NO_3]	1.49	2.20
SiO_2-[C_6mim][NO_3](50)	1.51	2.39
SiO_2-[C_{12}mim][NO_3](50)	1.05	2.04

[a]Standard uncertainty u are $u(CO_2)=0.03$ wt%

4.3 IL weight percentage (x)

The effect of IL-loading in gas adsorption capacities of SiO_2-IL(x) and (MCM-41)-IL(x) were studied and the results supported that by increasing the IL portion (x) in SiO_2-IL(x) and (MCM-41)-IL(x), the adsorption efficiencies decrease. As shown in Table 5, (MCM-41)-[C_6mim][NO_3](20) with 2.30 wt % and (MCM-41)-[C_6mim][NO_3](50) with 1.55 wt% had the highest and the lowest adsorption capacities. Similarly SiO_2-[C_{10}mim][NO_3](20) adsorbed about 1.88 wt% CO_2, but by increasing the IL's portion to 30, 40 and 50, the CO_2 adsorption capacities decreased to 1.68, 1.45 and 1.36 wt%, respectively (Fig. 8). This reduction was attributed to the occupation of more cavities in the sorbents with higher IL's portion.

Table 5 Effect of the ILs weight percentage (x) on CO_2 sorption capacity by passing dry CO_2 by a flow rate of 12 mL/min at 25 °C

Sorbents	CO_2 (wt%)[a]				
	x				
	0	20	30	40	50
SiO_2-[C_6mim][NO_3](x)	2.20	2.10	1.81	1.62	1.50
SiO_2-[C_8mim][NO_3](x)	2.20	2.07	–	–	1.47
SiO_2-[C_{10}mim][NO_3](x)	2.20	1.88	1.68	1.45	1.36
SiO_2-[C_{12}mim][NO_3](x)	2.20	1.59	1.28	1.16	1.05
(MCM-41)-[C_6mim][NO_3](x)	3.58	2.30	1.95	1.83	1.55
(MCM-41)-[C_{10}mim][NO_3](x)	3.58	2.44	–	–	1.42

[a]Standard uncertainty u are $u(CO_2)=0.03$ wt%

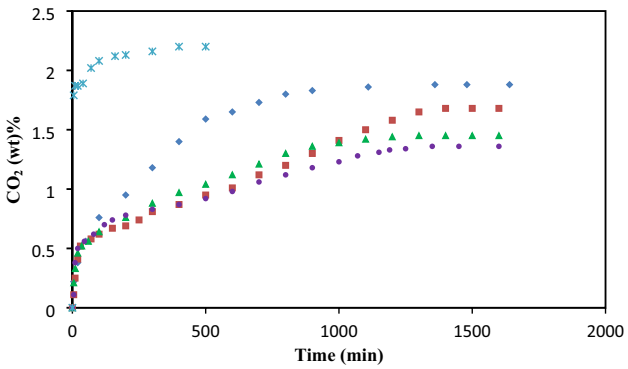

Fig. 8 CO_2 adsorption plot of SiO_2-[C_{10}mim][NO_3](x) with x = 0 (✳), 20 (◆), 30 (■), 40 (▲) and 50 (●) at 25 °C by passing dry CO_2 with a flow rate of 12 mL/min

4.4 CO_2 flow rate

There is an inverse relationship between the flow rate of the inlet gas and retention time of the gas in the reactor. This means that by an increase in the flow rate, the residence time reduces; i.e. the contact time of gas with the sorbent is shortened. Therefore, it is expected that by increasing the flow rate the sorption capacities would be decreased [20]. Experimental data confirm this claim. For instance, as shown in Table 6, by passing dry CO_2 at 25 °C with a flow rate of 12 mL/min, the absorption capacity of $[C_6mim][NO_3]$ was found to be 2.39 wt%, but with a rise in CO_2 flow rate to 25 and 50 mL/min, the absorption capacities reduced to 1.40 wt% and 0.81 wt%, respectively. This effect was also observed in solid sorbents. For example in (MCM-41)-$[C_6mim]$ $[NO_3](50)$, the CO_2 adsorption capacity at 25 °C and 12 mL/min flow rate was 1.55 wt%, but by increasing the flow rate to 25 and 50 mL/min, the weight gain reduced to 1.05 and 0.63 wt%, respectively.

5 Regeneration of saturated sorbents

In CO_2 sorption process, it is important to ensure the stability of the sorbents during the process. Doing so, the CO_2 sorption capacities of $[C_6mim][NO_3]$, SiO_2-$[C_6mim]$ $[NO_3](50)$ and (MCM-41)-$[C_6mim][NO_3](50)$ were measured by passing dry CO_2 through sorbents with a flow rate of 12 mL/min at 25 °C. Figure 9 shows the CO_2 sorption capacities of three sorbents during 8 desorption cycles. For example, the CO_2 absorption capacity of the neat $[C_6mim][NO_3]$ in Run 1 was 2.39 wt%, and with 3.77% reduction it dropped to 2.30% in Run 8. The same is also observed in other sorbents. The results indicated that the CO_2 adsorption capacities of SiO_2-$[C_6mim][NO_3](50)$ and (MCM-41)-$[C_6mim][NO_3](50)$ after 8 times ad/desorption, show about 5.34% and 5.17% decrease in adsorption, respectively.

Table 6 Effect of the flow rate on CO_2 sorption capacity at 25 °C

Sorbents	CO_2 (wt%)[a]		
	Flow rate (mL/min)		
	12	25	50
$[C_6mim][NO_3]$	2.39	1.40	0.81
SiO_2-$[C_6mim][NO_3](50)$	1.50	0.95	0.56
(MCM-41)-$[C_6mim][NO_3](50)$	1.55	1.05	0.63

[a]Standard uncertainty u are $u(CO_2) = 0.03$ wt%

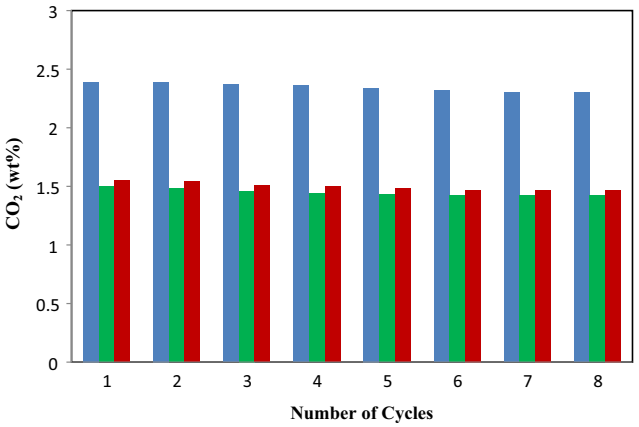

Fig. 9 Effect of recycle times on CO_2 sorption capacity of $[C_6mim][NO_3]$ (■), SiO_2-$[C_6mim][NO_3](50)$ (■) and (MCM-41)-$[C_6mim][NO_3](50)$ (■)

6 CO_2/N_2 selectivity

Given that N_2 has the highest mole fraction in air composition, it is important to clarify that the presence of N_2 can interfere or act as a barrier in CO_2 sorption. To shed light on this, the N_2 adsorption capacities of the bare and ILs-loaded silica or MCM-41 were studied under the conditions similar to those used for CO_2 adsorption experiments.

Table 7 Comparative gas adsorption capacity of the adsorbents by passing dry CO_2 and N_2 with a flow rate of 12 mL/min at 25 °C

Sorbents	CO_2 (wt%)[a]	N_2 (wt%)[a]	S_{CO_2/N_2}[b]
SiO_2 (amorphous)	2.20	0.21	10.5
MCM-41	3.58	0.77	4.7
SiO_2-$[C_6mim][NO_3](20)$	2.10	0.17	12.4
SiO_2-$[C_6mim][NO_3](30)$	1.81	0.12	15.1
SiO_2-$[C_6mim][NO_3](40)$	1.62	0.08	20.2
SiO_2-$[C_6mim][NO_3](50)$	1.50	0.06	25.0
SiO_2-$[C_{10}mim][NO_3](20)$	1.88	0.13	14.5
SiO_2-$[C_{10}mim][NO_3](30)$	1.68	0.09	18.6
SiO_2-$[C_{10}mim][NO_3](40)$	1.45	0.06	24.1
SiO_2-$[C_{10}mim][NO_3](50)$	1.36	0.05	27.2
(MCM-41)-$[C_6mim][NO_3](20)$	2.30	0.41	5.6
(MCM-41)-$[C_6mim][NO_3](30)$	1.95	0.28	7.0
(MCM-41)-$[C_6mim][NO_3](40)$	1.73	0.15	11.5
(MCM-41)-$[C_6mim][NO_3](50)$	1.55	0.09	17.2
(MCM-41)-$[C_{10}mim][NO_3](20)$	2.44	0.38	6.4
(MCM-41)-$[C_{10}mim][NO_3](50)$	1.42	0.07	20.3

[a]Standard uncertainty u are $u(CO_2) = 0.03$ (wt%), $u(N_2) = 0.01$(wt%)
[b]S_{CO_2/N_2} = selectivity of CO_2/N_2 (wt%)

Table 7 reveals that the bare SiO_2 and MCM-41 adsorb CO_2 about 10.5 and 4.7 times more than N_2, respectively, but due to the reduced surface area in SiO_2-ILs(x) and (MCM-41)-ILs(x) through impregnation, their CO_2 and N_2 adsorption capacities decrease. However, by an increase in the IL portion (x) in SiO_2-I(x) and (MCM-41)-IL(x), the CO_2/N_2 selectivity increases. For example, CO_2/N_2 adsorption ratio in SiO_2-[C_6mim][NO_3](20) was 12.4, but by the increase of x to 30, 40 and 50, the CO_2/N_2 selectivity increased to 15.1, 20.2 and 25, respectively. These results strongly suggest that SiO_2-IL(x) and (MCM-41)-IL(x) have greater tendencies to adsorb CO_2 than N_2, but the tendency in SiO_2-IL(x) is more than (MCM-41)-IL(x). For instance, the CO_2/N_2 selectivity in (MCM-41)-[C_6mim][NO_3](20) is about 5.6, but in SiO_2-[C_6mim][NO_3](20) is 12.4. The N_2 and CO_2 adsorption capacities of SiO_2-[C_{10}mim][NO_3](x) as well as CO_2/N_2 selectivity were drawn in Fig. 10.

7 CO_2 separation from its mixture with N_2

In order to examine whether SiO_2-ILs(x) adsorbents would be able to separate CO_2 from N_2/CO_2 mixtures, SiO_2-[C_6mim][NO_3](50) was used at 25 °C and atmospheric pressure, as the adsorbent in a bench scale. By using a set-up consisted of a series of four glass column reactors (height: 50 cm, diameter: 2 cm) filled with SiO_2-[C_6mim][NO_3](50), it was noticed that after 7 h pass of a CO_2/N_2 (20/80 vol%) stream with a flow rate of 2.5 L/h, the CO_2/N_2 composition of the gas stream exiting from the final glass reactor would become the same as the feed composition (CO_2/N_2 20/80). This would clearly support that SiO_2-[C_6mim][NO_3](50) has been saturated and needs to be recycled. The total SiO_2-[C_6mim][NO_3](50) used in the fourth glass reactors was 400 g. From a quantitative aspect, it could be concluded that by 7 h mix-gas passing (2.5 L/h flow rate), about 17.50 L gas would have passed through the sorbent, with the fractions for CO_2 and N_2 portions being 3.50 and 14 L, respectively.

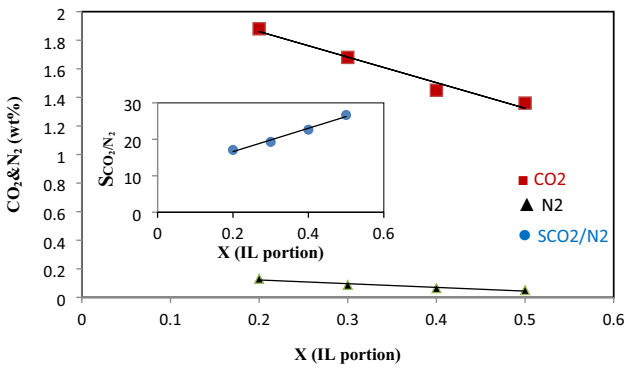

Fig. 10 The dependence plot of CO_2 (■) and N_2 (▲) adsorption capacity along with CO_2/N_2 selectivity (●) of SiO_2-[C_{10}mim][NO_3](x) *vs* IL's portion (x) at 25 °C by the pass of dry CO_2 & N_2 with a flow rate of 12 mL/min

8 Conclusion

The physical sorption capacities of the neat and solid supported [Rmim][NO_3] ionic liquids, where R was *n*-C_6H_{13}, *n*-C_8H_{17}, *n*-$C_{10}H_{21}$ and *n*-$C_{12}H_{25}$, respectively, were studied at different temperatures and flow rates by continuous passing the dry CO_2 or N_2 through physical sorbents. By passing dry CO_2 with a flow rate of 12 mL/min at 25 °C, [C_6mim][NO_3] had the highest absorption capacity among neat ILs. Increase in the temperature and flow rate caused an approximately linear decrease in absorption capacities. For example, by increasing temperature from 25 to 50 °C, the CO_2 absorption capacity in [C_6mim][NO_3] dropped from 2.39 to 1.28 wt%. In addition, by rising CO_2 flow rate from 12 to 50 mL/min, the absorption capacity reduced from 2.39 to 0.81 wt%. The ILs were immobilized via impregnation method onto mesoporous amorphous silica and high-ordered MCM-41 in different mole fractions. Due to higher surface area in MCM-41, the CO_2 and N_2 adsorption capacities of (MCM-41)-ILs(x) were higher than similar SiO_2-ILs(x). For instance, the CO_2 and N_2 adsorption capacities of SiO_2-[C_6mim][NO_3](20) were 2.10 and 0.17 wt%, respectively, while they were found to be 2.30 and 0.41 wt% in (MCM-41)-[C_6mim][NO_3](20), respectively. The results revealed that by an increase in IL's portion (x) in SiO_2-ILs(x) and (MCM-41)-ILs(x), their CO_2 and N_2 adsorption capacities decreased. whereas the CO_2/N_2 selectivity increased. For example, in SiO_2-[C_{10}mim][NO_3](50), the CO_2 adsorption capacity is 1.36 wt%, while by a decrease in IL's portion (x) to 40, 30 and 20, the adsorption capacities increased to 1.45, 1.68 and 1.88 wt%, respectively. However the CO_2/N_2 selectivity in SiO_2-[C_{10}mim][NO_3](20) was 14.5, but by the increase of x to 30, 40 and 50, the CO_2/N_2 selectivity raised to 18.6, 24.1 and 27.2, respectively. The CO_2/N_2 selectivity indicated that the SiO_2-IL(x) and (MCM-41)-IL(x) would be used for separation of CO_2 from N_2/CO_2 mixtures.

Supplementary Information The online version contains supplementary material available at https://doi.org/10.1007/s10934-023-01503-6.

Author contributions MM designed the project and supervised SHS, as M.Sc. student, carrying out all the experiments. MSA wrote the manuscript. AS was co-supervisor of the project and reviewed the manuscript text. All authors reviewed the manuscript.

Declarations

Conflict of interest The authors declare no conflict of interest.

References

1. D. Bonenfant, M. Mimeault, R. Hausler, Ind. Eng. Chem. Res. **42**, 3179 (2003)
2. F. Zhang, C.G. Fang, Y.T. Wu, Y.T. Wang, A.M. Li, Z.B. Zhang, Chem. Eng. J. **160**, 691 (2010)
3. J.P. Hallett, T. Welton, Chem. Rev. **111**, 3508 (2011)
4. L.A. Blanchard, D. Hancu, E.J. Beckman, J.F. Brennecke, Nature **399**, 28 (1999)
5. J.L. Anthony, J.L. Anderson, E.J. Maginn, J.F. Brennecke, J. Phys. Chem. B **109**, 6366 (2005)
6. S.G. Kazarian, B.J. Briscoe, T. Welton, Chem. Commun. **20**, 2047 (2000)
7. E.D. Bates, R.D. Mayton, I. Ntai, J.H. Davis, J. Am. Chem. Soc. **124**, 926 (2002)
8. M. Althuluth, J.P. Overbeek, H.J.V. Wees, L.F. Zubeir, W.G. Haije, A. Berrouk, C.J. Peters, M.C. Kroon, J. Membr. Sci. **484**, 80 (2015)
9. F. Kohler, D. Roth, E. Kuhlmann, P. Wasserscheid, M. Haumann, Green Chem. **12**, 979 (2010)
10. J. Ren, L. Wu, B.G. Li, Ind. Eng. Chem. Res. **51**, 7901 (2012)
11. J. Zhu, F. Xin, J. Huang, X. Dong, H. Liu, Chem. Eng. J. **246**, 79 (2014)
12. J. Ren, Z. Li, Y. Chen, Z. Yang, X. Lu, Chin. J. Chem. Eng. **26**, 2377 (2018)
13. M. Mirzaei, A.R. Badiei, B. Mokhtarani, A. Sharifi, J. Mol. Liq. **232**, 462 (2017)
14. M. Mirzaei, A.R. Badiei, B. Mokhtarani, A. Sharifi, Chem. Eng. Technol. **41**, 1272 (2018)
15. N.Y. Roik, L.A. Belyakova, J. Solid State Chem. **207**, 194 (2013)
16. P. Kubisa, Prog. Polm. Sci. **29**, 3 (2004)
17. L. Cammarata, S.G. Kazarian, P.A. Salter, T. Welton, Phys. Chem. Chem. Phys. **3**, 5192 (2001)
18. M.H. Valkenberg, C. deCastro, W.F. Holderich, Green Chem. **4**, 88 (2002)
19. W.L. Bragg, Scientia **23**, 153 (1929)
20. G. Severa, K. Bethune, R. Rocheleau, S. Higgins, Chem. Eng. J. **265**, 249 (2015)